Investigation of Massive MIMO Channel Spatial Characteristics for Indoor Subway Tunnel Environment

Asad Saleem and Yejun He*
Guangdong Engineering Research Center of Base Station Antennas and Propagation
Shenzhen Key Laboratory of Antennas and Propagation
College of Electronics and Information Engineering, Shenzhen University, 518060, China
Email: asadalvi64@yahoo.com and heyejun@126.com*

2021 Computing, Communications and IoT Applications (ComComAp) | 978-1-6654-2798-2/21/$31.00 ©2021 IEEE | DOI: 10.1109/COMCOMAP53641.2021.9652955

***Abstract*—Massive multiple-input multiple-output (MIMO) is perceived as an important technology for the fifth generation (5G) wireless communication networks because it employs large-scale antenna arrays to increase the network capacity, spatial characteristics, and throughput. For suburban line-of-sight (LoS) and non-line-of-sight (NLoS) environments, we investigate the angular spread of azimuth angle of departure (AoD), elevation angle of departure (EoD), azimuth angle of arrival (AoA), elevation angle of arrival (EoA), and channel condition number of the co-polarized and cross-polarized antenna systems. The study is based on the measurements conducted at the 3.5 GHz carrier frequency, 160 MHz bandwidth, and 32×64 cylindrical and planar antenna arrays. The Bartlett algorithm is used to jointly approximate the AoD, EoD, AoA, and EoA of the massive MIMO propagation channel. Results demonstrate that the MIMO channel characteristics show dependence with the antenna polarization combinations and angular spread drops rapidly as the distance between transmitter (Tx) and receiver (Rx) increases. Moreover, it is found that the co-polarized massive MIMO channel has a lower condition number and a higher capability to improve the system performance than the cross-polarized channels. The given results are extremely useful for antenna selection and analyzing the polarization-dependent massive MIMO system design.**

***Index Terms*—Multiple-input multiple-output system, Bartlett algorithm, delay spread, LTE systems, angular spread, and condition number.**

I. Introduction

Due to the few shortcomings of wireless local area networks in communication-based train control systems, the long-term evolution for metro (LTE-M) technology is known as the reliable communication solution for modern urban rail environments [1]. Rail transport systems have incorporated the 5G mobile communication based advance technologies, such as massive MIMO, to accommodate the high data rate requirements [2]. For the design of wireless communication systems and transmission technologies, it is required to investigate the propagation attributes of signals in various environments and to develop advanced wireless channel models [3]. As a result, the operators must need to investigate different propagation characteristics of 5G frequency bands (above 2 GHz) in the subway environment to establish advanced communication technologies and network architectures. The pioneering study [4] demonstrates that the multiple reflections and diffractions on the subway tunnel walls and shifts in the cross-sectional area result in a rather high diversity of the MIMO channel in subway tunnel scenario. Acknowledging the modal theory [5], the subway tunnel can be seen as a lossy waveguide, where the sum of active modes drops very quickly as the transceiver distance rises, limiting the degree of freedom (DoF) of the channel matrix in massive MIMO systems. However, when compared to a single-input single-output (SISO) channel, the channel capacity improvement is unusual. Based on the measurement campaign in the tunnel environment, the impact of space diversity, cross section, and polarization diversity of rectangular tunnel on the MIMO channel performance is studied in [6], which delivers solution for the optimal design of massive MIMO system in the tunnel environment. According to [7], a wideband SISO and 16 x 16 virtual MIMO testing campaign is considered in a two-dimensional 100 m long tunnel at a carrier frequency of 1.4725 GHz. The ray tracing method is used to explain the path loss, PDP, and RMS-DS characteristics, further it is revealed that the increment in the tunnel cross-section enhances the MIMO channel throughput.

In [8], the initial keyhole measurement campaign was implemented in the train-to-ground (T2G) communication environment, and it was revealed that the keyhole effect has a limited impact on the tunnel cross section and different polarization combinations. Bartlett's algorithm is one of the important angle of arrival (AoA) assessment technique and it provides each antenna element with an identical weighting to generate the steering vector in the desired direction [9]. This algorithm improves the antenna array radiations in the direction of arrival (DoA) by arranging the propagation delay of an incident signal, but the sources were propagating in other directions and the noise was not well handled. This algorithm gives poor assessment resolution, which relies basically on the size and structure of the antenna array. However, expanding the aperture structure leads to computational complexity increment and hardware issues. In [10], the Bartlett technique was considered to enhance the angular resolution of automobile radar system with a minimal number of antenna components by using linearly anticipated array expansion. In [11], the ray

tracing approach is used in the tunnel environment to predict radio signal propagation in the ultra-high-frequency band for vertical and horizontal polarized antenna arrays. It is revealed that within the subway tunnel, the high order power levels would be acquired if the horizontally polarized antennas are used, which is basically due to the variations in the reflection coefficients from the tunnel wall, especially in the segments where there exist no curvature part of the tunnel. Furthermore, the GSMA WRC Series specifications, such as 3.5 GHz, must be followed while configuring the 5G massive MIMO radio channels. However, the literature provides several studies on traditional MIMO systems, but many of these studies are lacking real-time tunnel characteristics and experimental recognition of the functional antenna placement. Therefore, more characterization of the massive MIMO channels is required from theory to practical applications in the tunnel environment.

In this paper, we study the massive MIMO channel spatial characteristics such as AoD, EoD, AoA, and EoA in both direct (LoS) and reflected (NLoS) scenarios by utilizing the horizontally and vertically polarized transceiver antenna arrays. To investigate the channel response over the apertures of the transmitter and receiver antenna arrays, we split the 32×64 sub-channels into two different polarization combinations such as co-polarized and cross-polarized. Furthermore, we estimate the power angular spectrum (PAS) by using the Bartlett beamforming technique and the channel condition number to estimate the capability of improving the channel capacity of massive MIMO radio channel. The major objective of this study is to figure out what polarimetric and geometrical elements might cause channel response variations in the presence of large-scale antenna arrays. The given results may be useful to create adaptive algorithms for adjusting array configurations to improve the system performance and channel capacity.

The remainder of this paper is structured in the following manner. To estimate the angular spread, Sect. II introduces the Bartlett beamforming method, measuring environment, and channel sounding. Sect. III presents the results and discussion. Finally, the conclusions are presented in Sect. IV.

II. Theoretical Analysis and Measurement Configuration

A. Bartlett Algorithm

To begin, the Bartlett beamforming technique is used to estimate the PAS from the original CIRs' received from measurements, i.e., direction-of-departure (DoD) and direction-of-arrival (DoA). The use of given algorithm is predicated on the supposition that the channel array response, also known as the steering vector $s(\theta, \varphi)$ which is determined in azimuth and elevation directions, is already known. The Bartlett beamforming algorithm is usually known as a Fourier spectrum analyzing approach. The aim is to discover the weighting vector w that maximizes the power of the received signals. The m-th order cylinderical antenna array elements can receive signals from the multiple spatially distributed users. Moreover, the received power is including both LoS path and reflected (NLoS) signals, which are apparently coming from various directions and arrival angles. Assume that the steering vector of the transmitted signals $x_1(t)$ from DoA is $s(\theta, \varphi) = [1, s_1(\theta, \varphi), s_2(\theta, \varphi), \ldots s_{\mathrm{m}-1}(\theta, \varphi)]^T$, where the phase shift and amplitude gain of a signal from the (ith+1) antenna number is denoted by $s_i(\theta, \varphi)$, and $(*)^T$ represents the transpose operator. For a uniform cylinderical array with m-th order elements and a radius ρ, the steering vector is formulated as

$$s(\theta, \varphi) = \left[e^{j\beta\rho \sin(\theta)\cos\left(\varphi - \frac{2\pi}{m}\right)}, \ldots, e^{j\beta\rho \sin(\theta)\cos\left(\varphi - \frac{(m-1)\times 2\pi}{m}\right)} \right]^T \quad (1)$$

where $\beta = 2\pi/\lambda$ represents the wave number. Moreover, the arrays' signal vector may be represented as:

$$y(t) = s(\theta, \varphi)x_1(t) + n(t) \quad (2)$$

where $n(t)$ represents the noise. Moreover, if there exist K sources with the same time slot and frequency, the received signals can be given as:

$$y(t) = \sum_{k=1}^{K} s(\theta, \varphi)x_k(t) + n(t) \quad (3)$$

Assuming that the received signal from azimuth direction, the output of Bartlett array can be measured as follows:

$$\max_{w} \mathrm{E}\left\{ w^{\mathrm{H}} y(\mathrm{t}) y^{\mathrm{H}}(\mathrm{t}) w \right\} = \max_{w} \mathrm{E}\left\{ \mathrm{x}(\mathrm{t})|^2 \left| w^{\mathrm{H}} x(\theta, \varphi) \right|^2 + \sigma^2 |w|^2 \right\} \quad (4)$$

where σ^2 represents the variance of a noise power and $(*)^H$ specifies the Hermitian transpose of the given vector. The significant solution of the Eq.1 can be written as:

$$w_B = \frac{s(\theta, \varphi)}{\sqrt{s(\theta, \varphi)^H s(\theta, \varphi)}} \quad (5)$$

where $s(\theta, \varphi)$ is a normalized vector, the weighting vector of Bartlett algorithm becomes:

$$w_B = s(\theta, \varphi)$$

This indicates that the weighting vector is identical to the spatial signature of the incident wave. The ultimate expressions for computing the PAS are only given here. Further information about the Bartlett algorithm can be acquired in [12]. The PAS of a considered $s(\theta, \phi)$ may be calculated as

$$P(\theta, \varphi) = \frac{s(\theta, \varphi)^H R_{xx} s(\theta, \varphi)}{s(\theta, \varphi)^H s(\theta, \varphi)} \quad (6)$$

where R_{xx} represents received signals covariance matrix and it can be estimated as

$$R_{xx} = \frac{1}{N \times M} \sum_{q=1}^{Q} \mathrm{vec}[Y(q)]\, \mathrm{vec}[Y(q)]^H \quad (7)$$

where $Y(q) \in C^{N \times M}$ represents the received signals at the $q-th$ delay-bin, $vec[.]$ shows the linear transformation operator which converts the matrix columns into a single column vector by following a sequential manner, M and N represent the number of receiver and transmitter antenna elements, respectively. If $s(\theta, \varphi)$ is the normalized vector, then the total PAS can be written as:

$$P(\theta, \varphi) = s(\theta, \varphi)^H R_{xx} s(\theta, \varphi) \quad (8)$$

TABLE I
MEASUREMENT PARAMETERS

Parameters	Description
Frequency	3.5 GHz
Transmitted Power	20 dBm
Polarization	Horizontal/Vertical
Bandwidth	160 MHz
Antenna Structure	Uniform Rectangular Array (Tx) / Uniform Cylinderical Array (Rx)
Tx/Rx Antennas Height	1.8 m/2.7 m
Total Distance for Measurements	500 m
SNR	20 dB
Tunnel Dimension	5.56 m (width)/5 m (height)/800 m (length)
Number of Sampling Locations	91

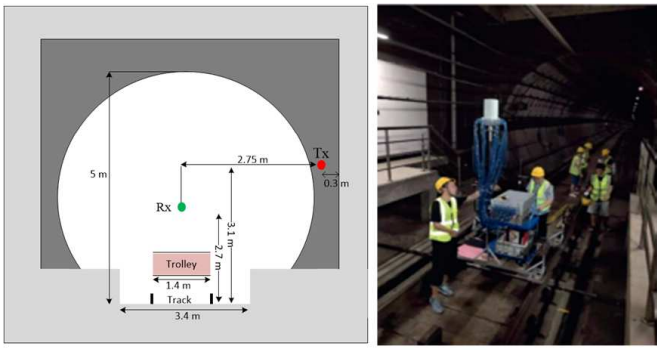

(a) (b)

Fig. 1. Measurement scenario, (a) Tunnel cross-sectional area, (b) Measurement campaign conducted in real tunnel environment.

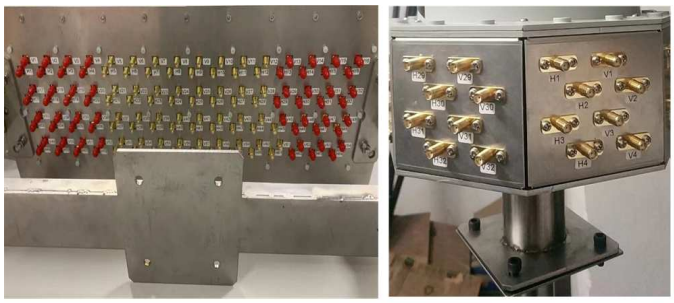

(a) (b)

Fig. 2. Antenna array structure used for the measurements: (a) Tx with rectangular array structure of 32 elements, (b) Rx with cylindrical array structure of 64 elements.

The following is the mathematical relationship for calculating the angular spread (AS) in [13]:

$$\bar{\theta} = \frac{\sum_{i=1}^{N} P_i \theta_i}{P} \tag{9}$$

$$\theta_{AS} = \sqrt{\frac{\sum_{i=1}^{N} P_i \left(\theta_i - \bar{\theta}\right)^2}{P}} \tag{10}$$

where P is the total received power at given measurement location, θ_i and P_i are the direction of departure/arrival and power of the $i-th$ path.

B. Measurement Environment and Setup Configuration

The metro Line 7 in Shanghai, P.R. China, is considered to perform measurement campaign between University Station and QiHua Rd. The tunnel has an arched cross section with a radius of 2.78 m, a bottom width of 3.4 m, and a height of 5 m (see Fig. 1(a)). The tunnel walls are reinforced with a concrete. The subway tunnel is separated into two distinct parts. The first is a 28.1 m long platform with the 5.55 m high rectangle-shaped cross-section. The other part is made up of non-platform components with a height of 4.96 m and arched cross sectional area. The longest distance between the transmitting and receiving antenna arrays in our wideband measurements is 800 m, however due to the subway's busy schedule, we are only able to measure the first 500 m. Within this 500 m long distance, total 91 different measurement locations are considered, whereas the initial 83 locations are equally separated from 10 m to 420 m with a uniform intervals of 5 m and the next 8 locations are separated by 10 m. The Tx antenna array is placed near to the tunnel wall to perform our measurement campaign and the Fig.1(b) depicts the inside view of the real subway tunnel. The access point receiver is mounted on a trolley that is traveling down the subway tunnel's central rail. The platform is 1.3 m high from the ground level, and the Tx is 1.8 m high from the platform level. By expanding the receiver height to 2.7 m, we minimized the impact of people executing the measurement campaign on the radio signal propagation.

For wideband channel measurements, the pseudo-noise sequence correlation technique (PN) is used. By using a Binary Phase Shift Keying (BPSK) property at the 3.5 GHz carrier frequency, a PN sequence is modulated with a 160 MHz bandwidth and 1023 chips length. To gather data in parallel, the receiver is splitted into 8 sub-channels. The transmitting and receiving antenna arrays structures are shown in Figs. 2(a) and 2(b). The received signal-to-noise ratio (SNR) is improved by using an amplifier. It should be noted, the static channel

TABLE II
ANGULAR SPREAD STATISTICAL PARAMETERS OF CO-POLARIZED AND CROSS-POLARIZED ANTENNA ARRAYS

	Co-Polarized			Cross-Polarized		
	Mean (°)	**Standard Deviation (°)**	**Maximum (°)**	**Mean (°)**	**Standard Deviation (°)**	**Maximum (°)**
ASD	7.78	10.92	68.06	4.69	9.50	64.73
ESD	2.21	2.69	16.35	4.25	3.67	16.76
ASA	5.14	4.37	23.88	7.06	3.89	18.71
ESA	6.07	2.83	12.42	5.45	2.33	11.66

calibration of 2048 (32×64) sub-channels may be performed in 20 ms, and each Rx position receives 128 cycles of measurement data. For the channel measurements, a massive MIMO channel sounder system is utilized. A rubidium clock is utilized to keep transmitting and receiving antenna arrays synchronized, and the total transmitted power is 20 dBm. On the Tx side, a rectangular antenna patch array (2×8) is placed. The uniform cylindrical antenna arrays on the receiving side is divided into eight parts, each with four vertically aligned antenna patches. For each cycle of channel sounding, 64 switching repetitions are performed at the Tx side to accomplish sequential switching. During a single transmission, data from eight different received channels may be acquired simultaneously on the Rx side, requiring only eight instances of switching to fulfill 64 receiving channels. For the initial 100 m (LoS route), the tunnel is straight, then curved for the leftover 700 m (NLoS path). On both the Tx and Rx sides, the antennas with directional patch arrays are considered for the channel measurements. The 3 dB beamwidth of antenna elements in the vertically and horizontally planes is 100° and 120°, respectively. All the multipath elements can be precisely separated in the tunnel scenario. The antenna patches in this system are separated by 0.5 λ, and each antenna pair consists of two co-located bi-polarized antennas (vertical and horizontal). Both antenna patches have two components, each with a polarization angle of ±45°. TABLE I contains an overview of the main measurement parameters.

III. Results and Analysis

The Power Delay Profile (PDP) describes how much power arrives at the receiver side with a certain delay [14], and may be calculated as $P(\tau)$ from the complex impulse responses $h(\tau)$. The PDP for the channels between the transceiver antennas is established by considering different polarization combinations and indexes are defined at certain delays (τ). By averaging the PDP statistics over the transceiver interface, the interference of small scale fading with the effective signal multipaths can be minimized. The PDP of the 32×64 measurement channels is shown in Fig. 3. From Fig. 3, we can distinguish between different power levels of sub-channels. The multipath components in PDP decay rapidly with time at 3.5 GHz. The excess delay ranges from 0 μs to 6.394 μs, with a fading range of [-44, 0] dB. For all channels, the power peaks occur between 2.385 μs to 4.479 μs delay. Some extra small peaks can be seen, which we believe are generated by the calibrated clock signals which are reflected from the ports. At low Tx-Rx distances, many propagation modes are activated. At a greater

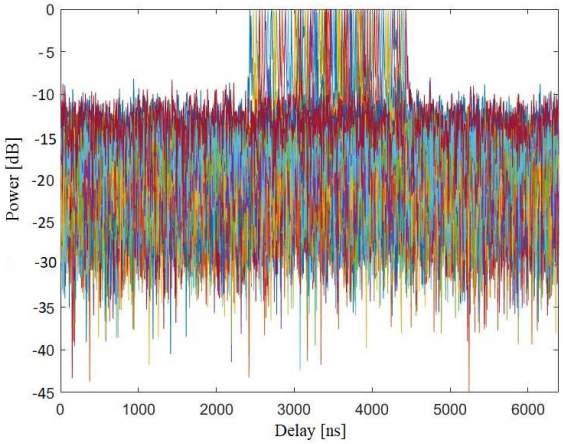

Fig. 3. The PDP of 32x64 massive MIMO sub-channels in tunnel environment.

distance, especially in the case of NLoS propagation scenario, model attenuation of high order becomes critical, and only the low order main model is retained. Thus, the reflected environment delay spread is rather constant and changes slowly. A path loss exponent of low order is established in the tunnel at given frequency band, but the subway tunnel still shows the waveguide phenomena. Furthermore, because the signal wavelength is shorter, it generates specular reflections, which further amplifies the waveguide effect in the given tunnel for high order frequency signals. When the tunnel sidewall blocks the multipath components, the waveguide effect is substantially diminished. Analyzing these propagation characteristics can assist in better understanding of the imbalanced channel properties.

The AS of co-polarized and cross-polarized transceiver antennas is calculated using the Bartlett method. It should be noticed that co-polarized antenna system can be demonstrated when both the transmitting and receiving antenna arrays are horizontally polarized and cross-polarized means when transmitting antenna array is horizontally polarized and receiving antenna array is vertically polarized. In Fig.4, ASD, ESD, ASA, and ESA are the AS of the azimuth angle of departure (AoD), the elevation angle of departure (EoD), the azimuth angle of arrival (AoA), and the elevation angle of arrival (EoA) for each receiving antenna location. Table II shows the AS statistical characteristics of co-polarized and cross-polarized transceiver antenna arrays. It can be observed that the angular spread drops very quickly as the distance between

TABLE III
STATISTICS OF CONDITION NUMBER

Poalrization	15 % [ns]	40 % [ns]	85 % [ns]	Mean [ns]	Standard Deviation [ns]
Co-Polarized	36.87	42.33	48.77	43.62	5.77
Cross-Polarized	40.09	46.61	54.69	47.28	6.71

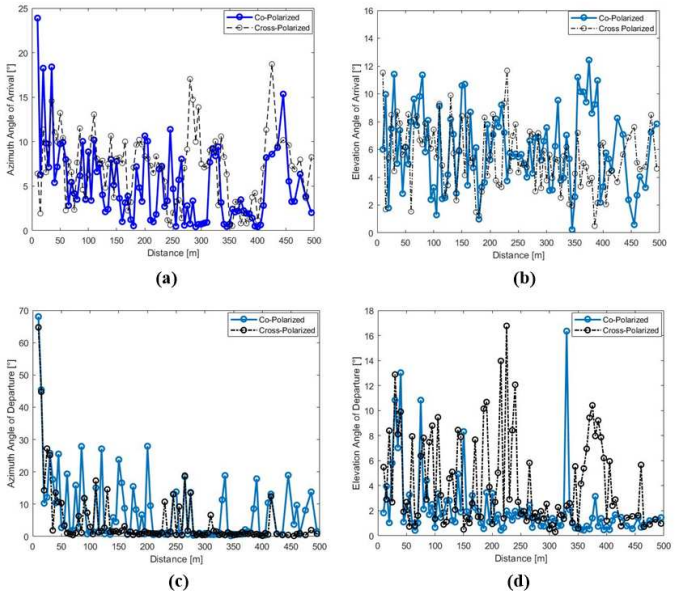

Fig. 4. Angular spread of co-polarized and cross-polarized antenna arrays at different locations for (a) ASA, (b) ESA, (c) ASD, and (d) ESD.

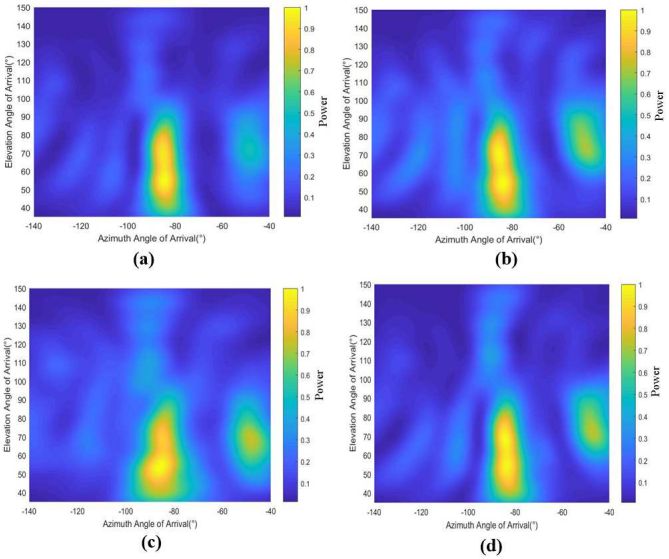

Fig. 5. Power angular spread of ASA and ESA at (a) 100 m for co-polarized antenna arrays, (b) 500 m for co-polarized antenna arrays, (c) 100 m for cross-polarized antenna arrays, and (d) 500 m for cross-polarized antenna arrays.

transmitting and receiving antennas increases. The ASA and ESD of co-polarized and cross-polarized antennas are found to be within 25° range. When the transceiver distance is between 180 m to 470 m, the ESD of cross-polarized is higher than that of co-polarized antenna arrays. This is due to the multipath components which are reflected many times in the curved part of the tunnel before arriving at the Rx, resulting in a rise of angular spread value. The ESD and ESA of cross-polarized and co-polarized are all within 17°. When the transceiver distance is less than 100 m, both co-polarized and cross-polarized ASA and ASD drop monotonously, where co-polarized antenna values are found smaller than the cross-polarized case. When the distance between the transmitter and the receiver is more than 100 m, the ESD and ESA of cross-polarized and co-polarized signals eventually become the same. They are practically the same until the transceiver distance reaches up to 180 m. It can be observed that the tunnel's curvature radius has a greater impact on the angular spread of azimuth angle than on the angular spread of elevation angle. Moreover, the reconstructed PAS using Bartlett approach for ASA and ESA at 100 m and 500 m distances for co-polarized and cross-polarized antenna arrays is shown in Fig.5. In the cross-polarization case, as shown in Fig.5, the PAS reproduces two main beams at 60° elevation and azimuths of −93° and −45° at 100 m and 500 m, respectively.

We use the condition number (CN) as a measure of massive MIMO system to ensure that the expected system can conceive 32×64 MIMO channel measurements. The mathematical relationship of the condition number is given by [15]

$$\gamma = 20 \log 10(\lambda_1/\lambda_2) \tag{11}$$

where $\lambda_1$and λ_2 are the highest and lowest eigenvalues of the MIMO channel matrix. A matrix with a low CN is regarded as a well-conditioned matrix, implying that the channel is in great capacity escalation shape. As a result, the value of CN may be used to check the channel characteristics. Because the coherent bandwidth of the channel is lower than the LTE-M signal bandwidth, we used wideband channel assumptions for the calibrations. The CN of co-polarized and cross-polarized transmitting and receiving antennas at various locations is shown in Fig.6(a). Moreover, the cumulative distribution function (CDF) of the condition number is shown in Fig.6(b). From Fig.6, it is clear that co-polarized system has lower condition number, so it has higher tendency to increase the system output than the cross-polarized antenna arrays. The cross-polarization coefficient increases in accordance to the incidence angle. However, the Brewster angle of the co-polarization coefficients specifies that they are always lesser than the cross-polarization coefficients. The incident ray at the tunnel ground and ceiling is perceived as horizontally polarized for co-polarized signals, whereas vertical polarization is detected at the tunnel side

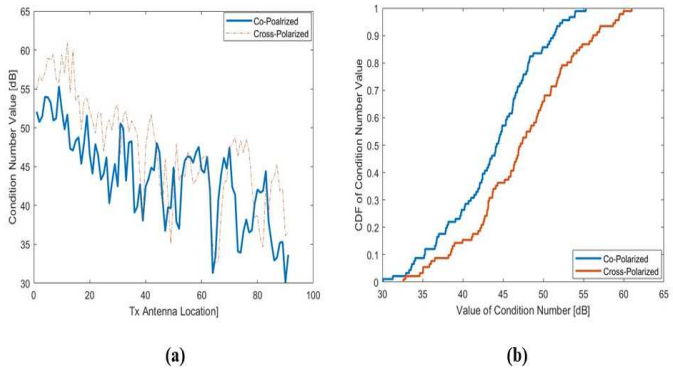

Fig. 6. The CN values for Co-Polarized and Cross-Polarized antenna arrays (a) at different receiving locations, (b) CDF of condition number.

walls. The inverse case is envisioned for the cross-polarized transmissions. By considering the reflection coefficients, the power of reflected rays from the tunnel walls is observed higher for co-polarization than the cross-polarization. Due to the tunnel width which is higher than the tunnel height, therefore the reflected signals from the tunnel side walls have a higher AoA than those with the tunnel ceiling and ground. Thus, the co-polarized signals have greater angular spread and a lower channel condition number than cross-polarized signals. The statistical results of co-polarized and cross-polarized antenna arrays for channel condition number are summarized in Table.III. The proposed study is quite useful to establish the optimal system design based on antenna placement and tunnel geometry influence on system performance. As a result, this article presents a prospective approach for LTE system design by considering the deployment of massive MIMO antenna structure in the tunnel environment.

IV. Conclusion

In this paper, a 32×64 massive-MIMO channel measurement campaign is introduced, which has been conducted in an indoor subway environment at the 3.5 GHz carrier frequency and the bandwidth of 160 MHz. We investigated the channel parameters such as power delay profile, angular spread of AoA, EoA, AoD, EoD, and the condition number in both LoS and NLoS situations for both the co- and cross-polarizations using the Bartlett method. The results demonstrate that the antenna configurations and polarization types have a large impact on the channel characteristics. When different antenna polarizations are used on the transmitting and receiving antenna sides, the arrival and departure angular properties (angular spread) are changed prominently. The condition number of co-polarization is found to be smaller than that of cross-polarization, which represents its ability to improve the channel capacity. Collectively, these findings offer guidance on the modeling of massive MIMO channel in indoor environments and will be helpful in designing of future LTE networks.

For future work, it would be useful to learn about diffraction and surface roughness impact on channel modeling. In addition, future research might cover the effects of diffraction and reflection on the radiated field, geometric-based stochastic modeling, as well as interference between antennas in massive MIMO systems.

Acknowledgment

This work is supported in part by the National Natural Science Foundation of China (NSFC) under Grants No. 62071306, and in part by Shenzhen Science and Technology Program under Grants JCYJ20200109113601723 and JSGG20210420091805014.

References

[1] W.K. Chiang and M.W. Wang, "Edge-Based Evolved Packet Core (EPC) Refactoring for High Speed Mobility," *SN Computer Science*, vol. 2, no. 5, pp. 1-26, Sep. 2021.

[2] L. Bai, Z. Huang, Y. Li, and X. Cheng, "A 3D Cluster-Based Channel Model for 5G and Beyond Vehicle-to-Vehicle Massive MIMO Channels," *IEEE Transactions on Vehicular Technology* , (Early Access), Jul. 2021.

[3] A. Tavsanoglu, C. Briso, D. Carmena-Cabanillas, R.B. Arancibia, "Concepts of Hyperloop Wireless Communication at 1200 km/h: 5G, Wi-Fi, Propagation, Doppler and Handover," *Energies* , vol. 14, no. 4, pp. 983, Jan. 2021.

[4] M. Lienard, P. Degauque, J. Baudet, and D. Degardin, "Investigation on MIMO channels in subway tunnels," *IEEE Journal on Selected Areas in Communications*, vol. 21, no. 3, pp. 332-339, Apr. 2003.

[5] J. Molina-Garcia-Pardo,M. Lienard,P. Degauque,D.G. Dudley, and L. Juan-Llacer, "Interpretation of MIMO Channel Characteristics in Rectangular Tunnels from Modal Theory," *IEEE Transactions on Vehicular Technology*, vol. 57, no. 3, pp. 1974-1979, May. 2008.

[6] R. Sun, Y. Lei, Z. Chen, and Z. Sun, "Investigation of MIMO Channel Characteristics in Tunnel at 1.4725 and 6 GHz," *Radio Science*, vol. 55, no. 10, pp. 1-1, Nov. 2020.

[7] R. Sun, D.W. Matolak, and C. Tao et al., "Investigation of MIMO Channel Characteristics in a Two-Section Tunnel at 1.4725 GHz," *International Journal of Antennas and Propagation*, vol. 2017, Article ID 3693149, 12 pages, Jul. 2017.

[8] J. Moreno Garcia-Loygorri, L. De Haro, C. Rodriguez, L. Cuellar, and J.M. Riera, "Influence of Polarization on Keyhole Probability on a MIMO-OFDM Train-to-Wayside System on Tunnels," *IEEE Antennas and Wireless Propagation Letters*, vol. 14, pp. 1798-1801, Apr 2015.

[9] MA.Al-Sadoon, RA. Abd-Alhameed, and NJ. McEwan, "The Impact of the Covariance Matrix Sampling on the Angle of Arrival Estimation Accuracy," *Inventions*, vol. 4, no. 3, pp. 43, Sep. 2019.

[10] H. Sim H, S. Lee,S. Kang, and SC. Kim, "Enhanced DOA Estimation using Linearly Predicted Array Expansion for Automotive Radar Systems," *IEEE Access*, vol. 7, pp. 47714-27, Apr. 2019.

[11] A. Saleem, F. Zhang, M. Wang, X. Yin, and G. Zheng G. "Proficiency of Leaky Coaxial Cable-Based MIMO System Using Radiated Field Distribution," *International Journal of Antennas and Propagation*, vol. 2018, Article ID 5016847, pages 13, Dec. 2018.

[12] N. Bailey and M. Bartlett, "An Introduction to Stochastic Processes: With Special Reference to Methods and Application." *Journal of the Royal Statistical Society. Series A (General)*, vol. 118, p. 484, Jan. 1955.

[13] J. P. Kermoal, L. Schumacher, K. I. Pedersen, P. E. Mogensen and F.Frederiksen, "A Stochastic MIMO Radio Channel Model with Experimental Validation," *IEEE Journal on Selected Areas in Communications*, vol. 20, no. 6, pp. 1211-1226, Aug. 2002.

[14] D. P. Gaillot, E. Tanghe, W. Joseph et al., "Polarization Properties of Specular and Dense Multipath Components in a Large Industrial Hall," *IEEE Transactions on Antennas and Propagation*, vol. 63, no. 7, pp. 3219-3228, Jun. 2015.

[15] Y. Hou, S. Tsukamoto, M. Ariyoshi, K. Kobayashi, and M. Okada, "2 by 2 MIMO System using Single Leaky Coaxial Cable for Linear-Cells," *In Proc. Personal, Indoor, and Mobile Radio Communication (PIMRC), 2014 IEEE 25th Annual International Symposium on*, pp. 327-331, Sep. 2014